Received: 28 December 2024 | Revised: 4 March 2025 | Accepted: 18 April 2025

DOI: 10.1111/jace.20610

Journal of the American Ceramic Society

RESEARCH ARTICLE

Enhanced domain dynamics in alternating current poled rhombohedral $Pb(Mg_{1/3}Nb_{2/3})O_3$–$PbTiO_3$ single crystals

Jeong-Woo Sun[1,2] | **Andrei Fluerasu**[3] | **Zhengze Xu**[2] | **Sipan Liu**[2] | **Sang-Goo Lee**[4] | **Wook Jo**[1] | **Xiaoning Jiang**[2] | **Jong Eun Ryu**[2]

[1]Department of Materials Science and Engineering, Ulsan National Institute of Science and Technology, Ulsan, Republic of Korea

[2]Department of Mechanical and Aerospace Engineering, North Carolina State University, Raleigh, North Carolina, USA

[3]National Synchrotron Light Source II (NSLS-II), Brookhaven National Laboratory, Upton, New York, USA

[4]iBULe Photonics, Inc., Yeonsu-gu, Incheon, Republic of Korea

Correspondence
Jong Eun Ryu, Department of Mechanical and Aerospace Engineering, North Carolina State University, Raleigh, NC 27695, USA.
Email: jryu@ncsu.edu

Funding information
Brookhaven National Laboratory, Grant/Award Number: DE-SC0012704; Defense Acquisition Program Administration, Grant/Award Number: R230102; Office of Naval Research, Grant/Award Number: N00014-21-1-2058; National Science Foundation, Grant/Award Number: DMR-2309184

Abstract

The understanding of domain dynamics in ferroelectric materials is crucial for optimizing their performance in piezoelectric and electro-optic applications. Although previous studies have focused on static domain structures and macroscopic characteristics, the time-resolved approach of domains remains largely unexplored. In this study, we compare the dynamic responses of direct current (DC) and alternating current (AC) poled [001]-oriented rhombohedral $Pb(Mg_{1/3}Nb_{2/3})O_3$–$PbTiO_3$ (PMN–PT) single crystals using X-ray photon correlation spectroscopy (XPCS) during the application of external electric fields. Our results demonstrate that the AC-poled sample exhibit enhanced reconfiguration of domain variants in response to driving fields compared to the DC-poled counterpart, as evidenced by accelerated correlation decay and faster relaxation time. This phenomenon is attributed to enhanced reversible domain wall motion achieved through AC poling, which facilitates field-induced domain realignment. These findings provide insight into the relationship between dynamics and macroscopic properties in relaxor-PT single crystals for high-performance applications.

KEYWORDS

AC poling, domain dynamics, piezoelectricity, PMN–PT single crystals, X-ray photon correlation spectroscopy

1 | INTRODUCTION

Ferroelectric materials possess unique switchable polarization characteristics, which have driven significant advancements in advanced piezoelectric and electro-optic applications.[1,2] The functional properties of ferroelectrics are inherently linked to their domain configurations.[3] In the virgin state, ferroelectric domains are disordered, resulting in canceled macroscopic effects due to random orientations.[4] Through electrical poling, where an external electric field aligns the domains, the materials can acquire remanent polarization (P_r), leading to enhanced

dielectric and electromechanical responses.[5,6] Therefore, engineering the domain structure has become crucial for optimizing the performance of ferroelectric systems.

Research on ferroelectric domains has primarily focused on static measurements of crystallography and domain configurations to analyze the relationship between poling and macroscopic properties.[7] Particularly, the alternating current (AC) electric field poling technique in [001]-oriented rhombohedral relaxor-$PbTiO_3$ single crystals has been shown to produce higher dielectric and piezoelectric properties compared to direct current (DC) poling method.[8,9] To date, various approaches such as phase-field simulation and phenomenological analysis have investigated the enhanced performance after AC poling, attributed to reduced 71° domain walls and striped 109° domain walls with larger domain sizes.[10–13] Furthermore, AC-poled crystals exhibit a lower coercive field (E_C) than DC-poled specimens, suggesting that AC poling induces softer characteristics as the required Gibbs free energy for polarization reversal decreases, accounting for the decreased E_C.[14,15] It is notable that small-signal properties in AC-poled samples show a more pronounced peak at the phase transformation temperature than DC-poled counterparts,[16] which indicates different dynamic behavior. Nevertheless, systematic research on the analysis of time-resolved domain dynamics during applied external driving stimuli is still limited, impeding the further characterization and design of relaxor ferroelectric single crystals.

Here, we employ in situ X-ray photon correlation spectroscopy (XPCS) to investigate the dynamic behavior of [001]-poled rhombohedral $Pb(Mg_{1/3}Nb_{2/3})O_3$–$PbTiO_3$ (PMN–PT) single crystals under applied electric fields.[17] The coherent scattering generates speckle patterns with intensity variations that capture spatial information in reciprocal space. XPCS provides a unique capability to capture domain dynamics with high temporal resolution by analyzing electric field-driven changes of the speckle topology. By examining dynamic properties, we aim to determine whether the enhanced properties of the AC-poled sample are related to more responsive dynamics than the DC-poled counterpart. Our investigation reveals that the AC-poled sample shows enhanced realignment of domain variants in response to driving fields compared to the DC-poled crystal. This enhanced dynamic behavior is evidenced by accelerated correlation decay and increased reversible domain wall motion.

2 | MATERIALS AND METHODS

Single crystals of [001]-oriented rhombohedral PMN–29PT were manufactured from iBULe Photonics Co. Ltd using the Bridgeman technique. The crystals were cut into samples with dimensions of 3 mm × 3 mm × 1 mm, followed by the deposition of Ti/Au (10 nm/100 nm) electrodes on the [001] surfaces (3 mm × 3 mm) through sputtering to enable electrical connections. Prior to poling procedures, all specimens underwent thermal depolarization at 250°C for 30 min.[5] At room temperature (25°C), two distinct poling processes were implemented using a function generator (Agilent Technologies, 33250A, Santa Clara, CA, USA) and a high-voltage amplifier (Electrical Energy Limited, EEL1102.05, Barker, NY, USA) in a silicone oil-filled fixture. DC poling involved applying a constant electric field of 5 kV/cm for 60 s, whereas AC poling employed a bipolar triangular waveform with a peak-to-peak amplitude of 10 kV_{pp}/cm for 20 cycles at 1 Hz.[8] The dielectric permittivity (ε_r) of poled samples were characterized using a multi-frequency LCR meter (Agilent Technologies, 4294A, Santa Clara, CA, USA) at 1 kHz. The longitudinal piezoelectric coefficients (d_{33}) were measured using a quasi-static piezo d_{33} meter (Model ZJ-4B, Chinese Academy of Science, China).

XPCS measurements were performed at the Coherent Hard X-ray Scattering (CHX) beamline at NSLS-II, Brookhaven National Laboratory. The experimental setup utilized a 12.8 keV coherent X-ray beam, achieving an attenuation length of approximately 25 μm. Beam focusing was accomplished through a combination of beryllium compound refractive lenses and silicon kinoform lenses. Scattering patterns were recorded using a 2D Eiger X 1 M detector with 75 × 75 μm^2 pixels covering an active area of 1030 × 1065 pixels, positioned 1.5 m from the specimen. The scattering vector (Q) was determined as $Q = k_{out} - k_{in}$, where k_{in} and k_{out} represent the incoming and outgoing wave vectors, respectively. k_{in} was oriented along the y-axis, with a magnitude determined by the X-ray wavelength λ as $|k_{in}| = 2\pi/\lambda$. For each detector pixel (i, j), the coordinates $x = (i - x_0) \cdot p$ and $y = (j - y_0) \cdot p$ were calculated relative to the beam center, where p is the pixel size and (x_0, y_0) denotes the beam center. The scattering angle (2θ) was obtained as $\tan(2\theta) = \sqrt{x^2 + y^2}/D$, and the azimuthal angle Ø as $\arctan(y/x)$, where D is the sample-to-detector distance. The k_{out}, which shares the same magnitude as k_{in}, points in the direction specified by these angles. In reciprocal space mapping, 2D images were collected with Q_x representing the parallel component and Q_z the perpendicular component relative to the sample surface. A region of interest (ROI) was carefully selected from areas exhibiting high signal-to-noise ratios to differentiate sample speckles from background signals at the sub-micron scale. To investigate domain dynamics, three different electric fields of increasing field, step-increasing field, and 5-times unipolar triangular waveform (Figure S1), were applied using the same func-

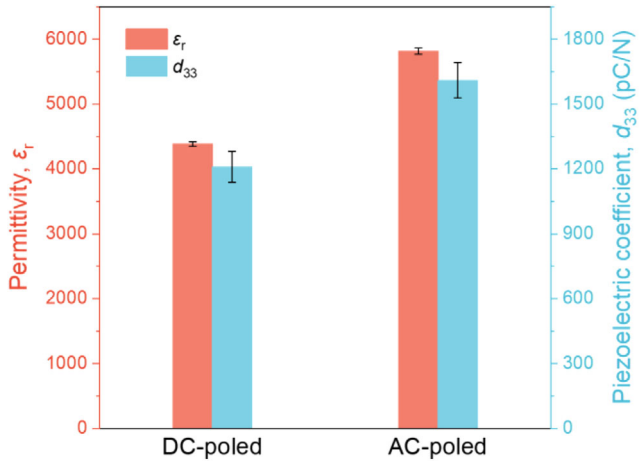

FIGURE 1 Relative permittivity (ε_r) and longitudinal piezoelectric coefficient (d_{33}) for DC-poled and AC-poled PMN–PT single crystals. AC, alternating current; DC, direct current.

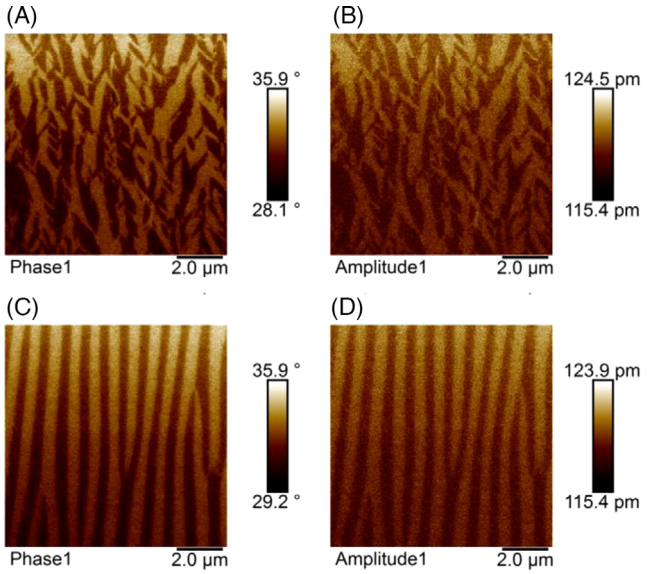

FIGURE 2 Piezoresponse force microscopy (PFM) images representing out-of-plan domain configurations in (a, b) DC-poled, and (c, d) AC-poled samples with phase and amplitude contrast.

tion generator and high voltage amplifier in the poling processes. These fields were applied in alignment with the initial poling state to prevent polarization reversal during measurement. For each measurement condition, speckle patterns were recorded at room temperature, collecting 300 patterns with both acquisition and exposure times of 1 s. Time-resolved correlation analysis was performed on the speckle patterns to evaluate dynamics and response characteristics under the various field conditions.

3 | RESULTS AND DISCUSSION

A comparative analysis of dielectric and piezoelectric properties between [001]-oriented DC-poled and AC-poled rhombohedral PMN–PT single crystals reveals significant difference in Figure 1. The AC-poled crystals demonstrate enhanced properties, exhibiting a relative permittivity (ε_r) of approximately 5800 compared to 4400 in DC-poled samples. Similarly, AC-poled crystals show an increased piezoelectric coefficient (d_{33}) of ~1600 pC/N, whereas DC-poled specimens achieve ~1200 pC/N. Previous studies using piezoresponse force microscopy (PFM),[18] polarization light microscopy (PLM),[14,19] and phase-field simulation[12] have established that domain configurations undergo distinct changes after DC and AC poling, which can lead to varying dynamic behaviors in different domain structures. Figure 2 shows different domain structures in DC-poled and AC-poled samples. PFM images before poling are also presented in Figure S2. The AC-poled sample exhibits larger domain sizes than its DC-poled counterpart. In the DC-poled crystal, both 109° and 71° domain walls are clearly distinguishable, forming a 4R domain configuration. Conversely, the AC-poled specimen exhibits prominent 109° domain walls that create a lamellar domain structure, whereas the 71° domain walls become less pronounced, resulting in a 2R configuration.[11,12] To verify the property enhancement and dynamic behavior of AC-poled crystals, XPCS was utilized to investigate domain dynamics under external electric fields.

In Figure 3, speckle patterns emerge from coherent X-ray scattering through inhomogeneous regions of the samples. The experimental setup yields a single-pixel reciprocal space coverage (ΔQ_{PIX}) of approximately 3.24×10^{-4} Å^{-1}, and the total reciprocal space coverage (ΔQ_{DET}) extends to about 0.345 Å^{-1}. These measurements in reciprocal space correspond to real space modulations where the largest detectable features (Δl_{PIX}) are approximately 19.4 μm, and the smallest observable modulations (Δl_D) are around 18.2 nm. From this respect, the speckle patterns can represent the modulation of ferroelectric domains at mesoscales. The DC-poled and AC-poled specimens exhibit distinct differences in their speckle pattern, which are represented by a color gradient from purple (lowest intensity) to yellow (highest intensity). The DC-poled sample in Figure 3a shows a more diffuse pattern with less intense yellow regions and a broader distribution of intensities. In contrast, the AC-poled crystal in Figure 3b displays a more concentrated and intense speckle pattern characterized by a smaller yellow central region. Due to the inverse relationship in reciprocal space, AC-poled samples exhibit larger real-space domains. Their increased domain sizes are evidenced by narrower speckle intensities and PFM images compared to DC-poled counterparts (Figure 2).[20]

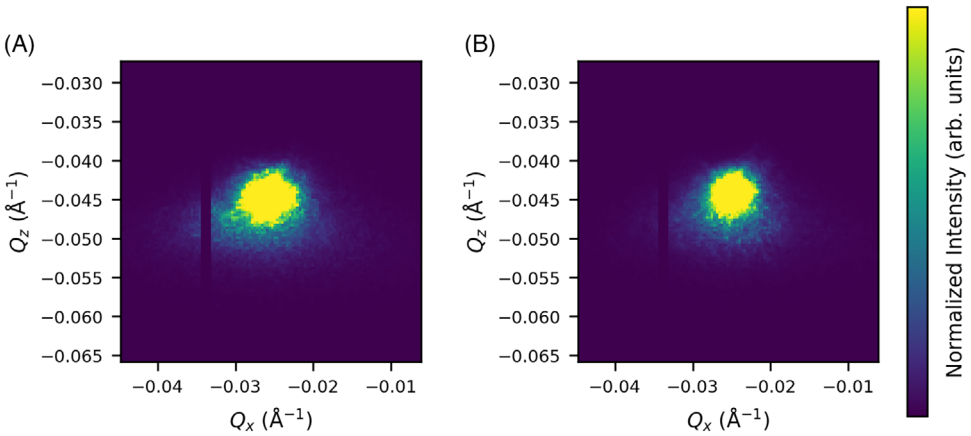

FIGURE 3 Speckle patterns of (a) DC-poled and (b) AC-poled rhombohedral PMN–29PT single crystals using X-ray photon correlation spectroscopy (XPCS).

The dynamic analysis employs a correlation coefficient (C) to quantify the relationship between pairs of speckle patterns A and B,

$$C(A,B) = \frac{\Sigma_m \left(A_m - \bar{A}\right)\left(B_m - \bar{B}\right)}{\sqrt{\Sigma_m \left(A_m - \bar{A}\right)^2 \Sigma_m \left(B_m - \bar{B}\right)^2}}, \quad (1)$$

where A_m and B_m represent the intensities recorded at pixel m, $\bar{A}$ and $\bar{B}$ denote the average intensities of their respective patterns.[21] In Figure S3, the consistent color in two-time correlation plots confirms no significant domain reorientation or dynamics occurred in the absence of an applied electric field. It is noteworthy that the domain structures remained static, less affected by beam-induced effects or spontaneous fluctuations. This result confirms that correlation behaviors observed during the 300-s XPCS measurements under applied electric fields can be directly attributed to the external field effects, rather than to inherent sample dynamics or experimental artifact.

The dynamic behavior of domains in DC-poled and AC-poled PMN–PT single crystals was investigated using two-time correlation analysis under applied increasing electric fields, as shown in Figure 4. The correlation maps present a color scale that represents the degree of correlation between speckle patterns at two time points (t_1 and t_2), with red indicating high correlation and blue indicating low correlation. In Figures 4a,b, both DC-poled and AC-poled samples exhibit distinctive correlation patterns under the increasing electric field. The AC-poled sample demonstrates more pronounced changes characterized by broader and more intense blue regions, indicating more significant domain evolutions and higher dynamic activity than the DC-poled counterpart.[22] The quantitative comparison of dynamics is illustrated in Figure 4(c), which shows the evolution of the correlation coefficient as a function of time during applied electric field. The analysis utilizes the Kohlrausch–Williams–Watts (KWW) stretched exponential model, which is employed to empirically characterize the correlation decay as a function of time (t): $\exp(-(\frac{t}{\tau})^{\beta})$, where τ represents the relaxation time and β is the shape parameter indicating the degree of deviation from an exponential function.[23,24] Both poled samples show an initial correlation coefficient of 1.0 that reduces with increasing fields, which indicates domain reorganization. When a unipolar electric field is applied to a poled material in the same direction as the original poling field, domain reconfiguration occurs through alignment of back-switched domains after the initial poling.[4,25] Notably, the AC-poled specimen exhibits a faster decay rate with approximately 21% lower τ than the DC-poled counterpart, indicating more domain alignment along the electric field in the AC-poled crystal. In Figure S4, we observe small differences between DC-poled and AC-poled samples in correlation decay below the coercive field (E_C). However, significant discrepancies emerge above the E_C, where sufficient energy becomes available to overcome local constraints such as internal stress and electric field. This enables rearrangement of domain variants, resulting in more pronounced drops in correlation coefficients for the AC-poled crystal. For the dielectric response upon unipolar field application in ferroelectrics, two reversible contributions have been identified.[26] The first arises from the intrinsic piezoelectric effect, specifically lattice distortion of the crystallographic unit cell. The second is extrinsic reversible domain wall motion, characterized by a small shift of domain walls from their equilibrium positions without leaving their potential minima.[27] Previous studies have shown that extrinsic reversible domain wall motion is the primary contributor to the high piezoelectricity, whereas the intrinsic

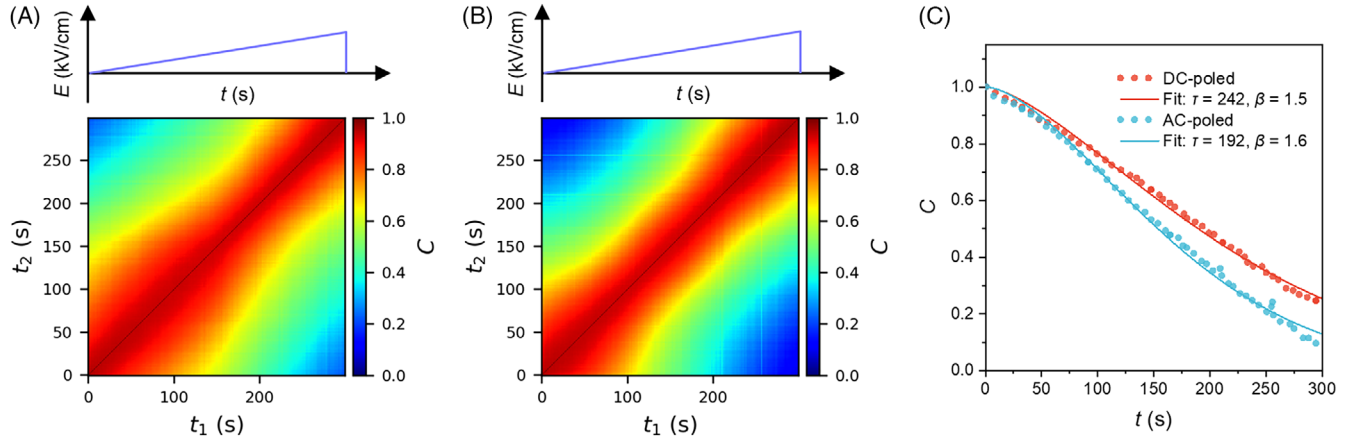

FIGURE 4 Two-time correlation analysis of (a) DC-poled and (b) AC-poled samples under an increasing electric field up to 5 kV/cm for 300 s. (c) Time-dependent correlation coefficient showing correlation decay dynamics as a function of time during applied electric field. The two-time correlation plot quantifies speckle fluctuations between two time points t_1 and t_2. The color bar represents the correlation coefficient (C) ranging from 1 (red, indicating identical speckle patterns) to 0 (blue, indicating completely uncorrelated speckle patterns).

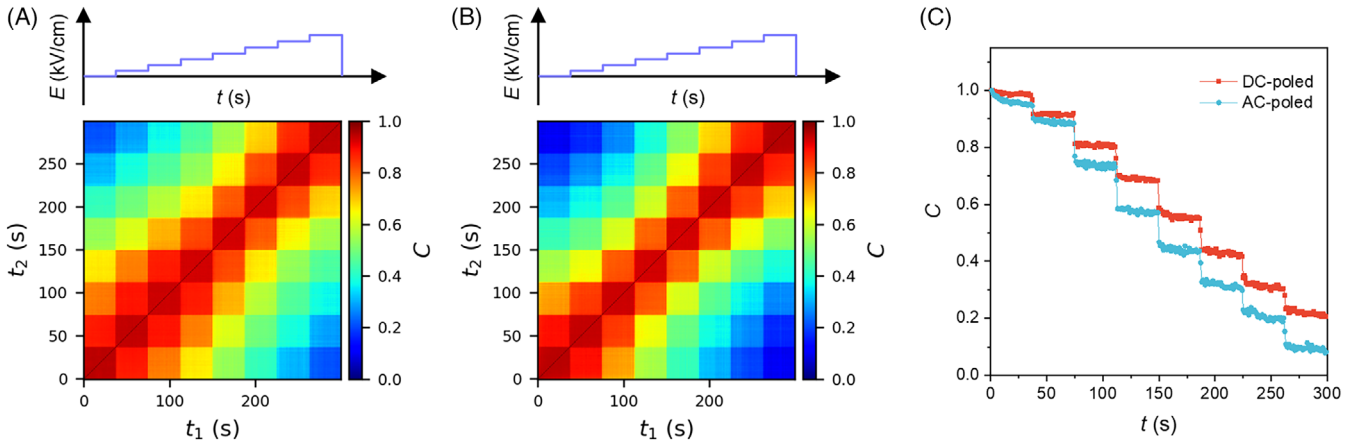

FIGURE 5 Two-time correlation analysis of (a) DC-poled and (b) AC-poled specimens under a step-increasing electric field up to 5 kV/cm for 300 s. (c) Time-dependent correlation coefficient showing correlation decay dynamics as a function of time during applied electric field.

contribution from lattice deformation accounts for only a small portion of the enhanced performance.[28–30] Furthermore, [111]-oriented rhombohedral PMN–PT single crystals are dominated by intrinsic piezoelectric effects due to its single-domain state, whereas [001]-oriented rhombohedral PMN–PT crystals exhibit approximately 15 times larger unipolar strain through activated non-180° domain wall motion that would facilitate reversible domain wall movement.[31,32] Therefore, the increased responsiveness to external driving fields observed in AC-poled crystals can be attributed to enhanced domain wall motion, which enables accelerated correlation decay dynamics.

Figure 5 demonstrates the temporal evolution of domain dynamics under step-increasing electric fields. In Figure 5a,b), the two-time correlation maps reveal that the diagonal checkerboards directly correspond to each step increase in the electric field. These distinct bands indicate periods of relative stability between field increments, where domain configurations show temporarily little change. The width of these diagonal bands represents the duration of each electric field step, whereas the sharp transitions between them (represented by distinct color changes) coincide with the moments of field increase. Both samples show stronger decorrelation at higher time differences, indicating that topological evolutions become more pronounced as the field strength increases. This step-dependent behavior is more evident in the AC-poled crystal, where the greater contrast is shown far from the diagonal. Figure 5c indicates the step-response behavior, with each downward step in the correlation

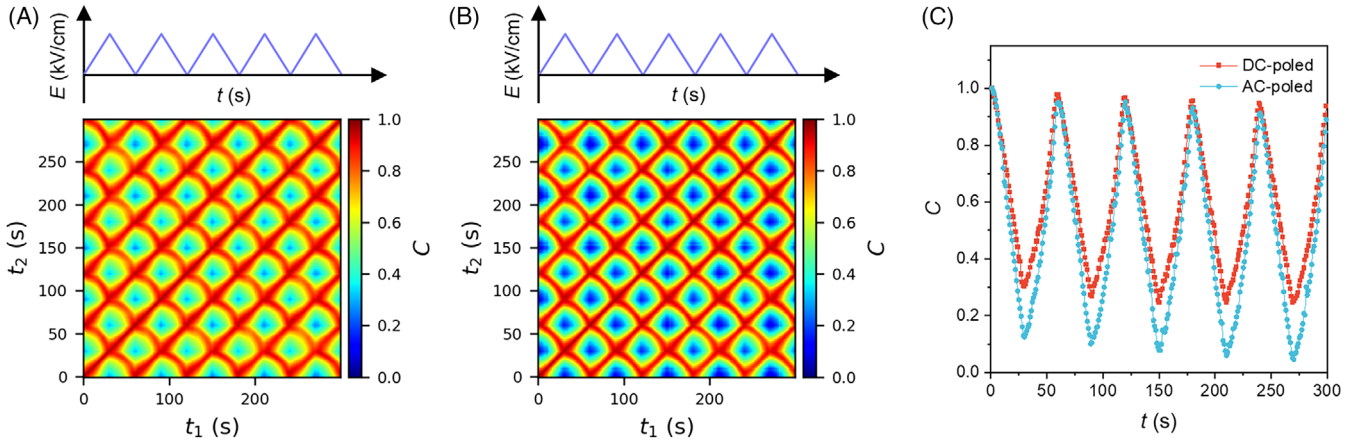

FIGURE 6 Two-time correlation analysis of (a) DC-poled and (b) AC-poled samples under a 5-cycle unipolar triangular waveform up to 5 kV/cm for 300 s. (c) Time-dependent correlation coefficient showing dynamic fluctuations as a function of time during applied electric field.

coefficient corresponding to a field increment. The stairstep pattern shows that each field increase triggers a discrete dynamic behavior in domain configuration. Under weak and subswitching fields (below 0.7 kV/cm), both DC- and AC-poled samples show similar correlation drops, indicating that the applied energy is insufficient to overcome the threshold required for significant domain reorganization.[33] At higher fields above the E_C, the AC-poled sample shows larger correlation drops compared to the DC-poled counterpart. This difference suggests that the AC-poled configuration facilitates domain reconfiguration with increased realignment and enhanced correlation change. Furthermore, the AC-poled crystal can show enhanced domain wall motion under external electric fields in agreement with Figure 4. [34]

In Figure 6, the correlation maps reveal periodic patterns under cyclic unipolar electric field application. Figure 6a,b show distinct patterns in both correlation maps demonstrate the reversible effect of domain responses over five complete field cycles. The AC-poled specimen exhibits more intense color contrast with alternating red and blue regions, signifying larger fluctuations in domain reorganization during each field cycle compared to the DC-poled counterpart. Figure 6c illustrates the cyclic behavior of the correlation coefficient, with both samples showing five oscillations corresponding to the five field cycles. The correlation coefficient presents around 1.0 when the applied field is close to zero and fluctuates as the field increases or decreases. The return to high correlation values after each field cycle confirms the reversible process of domain realignment, indicating that the heterogeneous speckle topology returns to approximately the original positions upon field removal. The increased amplitude of correlation coefficient in the AC-poled sample indicates more reconfiguration of reversible domain variants than the DC-poled crystal.[35] Given that the piezoelectric response is thought to be a small portion as discussed in Figure 4, this result supports that displacement of domain walls is reversible under external unipolar fields. The domain wall will return to the former equilibrium position when the driving field is removed,[27] and similar behavior is observed with 5-times unipolar sinusoidal electric fields (Figure S5). Hence, the greater magnitude of oscillations suggests that the AC-poled configuration exhibits improved reversible domain wall motion, contributing to superior dynamic characteristics and enhanced properties.

4 | CONCLUSIONS

We investigated domain dynamics under applied external fields by comparing DC-poled and AC-poled samples of [001]-oriented rhombohedral PMN–PT single crystals using XPCS correlation analysis. The results demonstrated that AC poling induces enhanced dynamic behavior compared to DC poling. The AC-poled sample showed enhanced domain dynamics, characterized by faster relaxation time and greater correlation decay when subjected to external electric fields. This behavior suggests more realignment of domain variants in the AC-poled crystal, which contributes to its improved reversible domain wall motion compared to the DC-poled counterpart. Our study provides valuable insights into the relationship between dynamics and macroscopic performance in relaxor ferroelectric single crystals for piezoelectric applications.

ACKNOWLEDGMENTS

This work was supported by NSF under Grant no. DMR-2309184. ZX and XJ also acknowledge the support from ONR under Grant no. N00014-21-1-2058. This research used resources, 11-ID CHX beamline, of the National Syn-

chrotron Light Source II, a U.S. Department of Energy (DOE) Office of Science User Facility operated for the DOE Office of Science by Brookhaven National Laboratory under Contract No. DE-SC0012704. This work was supported by Korea Research Institute for defense Technology planning and advancement through Defense Innovation Vanguard Enterprise Project, funded by Defense Acquisition Program Administration (R230102).

CONFLICT OF INTEREST STATEMENT

The authors declare no conflicts of interest.

ORCID

Jeong-Woo Sun https://orcid.org/0000-0003-1018-5363
Wook Jo https://orcid.org/0000-0002-7726-3154

REFERENCES

1. Jo W, Dittmer R, Acosta M, Zang J, Groh C, Sapper E, et al. Giant electric-field-induced strains in lead-free ceramics for actuator applications—status and perspective. J Electroceram. 2012;29:71–93.
2. Zhang Y, Jie W, Chen P, Liu W, Hao J. Ferroelectric and piezoelectric effects on the optical process in advanced materials and devices. Adv Mater. 2018;30:1707007.
3. Sun JW, Xu Z, Lee SG, Jo W, Jiang X, Eun Ryu J. A review of experimental methods for characterizing ferroelectric domain dynamics in relaxor-$PbTiO_3$ single crystals. IEEE Trans Ultrason Ferroelectr Freq Control. 2025;72:2–19.
4. Dragan D. Ferroelectric, dielectric and piezoelectric properties of ferroelectric thin films and ceramics. Rep Prog Phys. 1998;61:1267.
5. Sun JW, Choi WJ, Yu HL, Lee SG, Ryu JE, Zate TT, et al. Enhanced polarization retention and softening in [001]-oriented $Pb(Mg_{1/3}Nb_{2/3})$–$PbTiO_3$ single crystals through corona poling. J Korean Ceram Soc. 2024;61:854–60.
6. Haertling GH. Ferroelectric ceramics: history and technology. J Am Ceram Soc. 1999;82:797–818.
7. Zhang S, Li F. High performance ferroelectric relaxor-$PbTiO_3$ single crystals: status and perspective. J Appl Phys. 2012;111:031301.
8. Kim HP, Wan H, Luo C, Sun Y, Yamashita Y, Karaki T, et al. A review on alternating current poling for perovskite relaxor-$PbTiO_3$ single crystals. IEEE Trans Ultrason Ferroelectr Freq Control. 2022;69:3037–47.
9. Sun Y, Karaki T, Yamashita Y. Recent progress on AC poling of relaxor-$PbTiO_3$ ferroelectric single crystals: a review. Jpn J Appl Phys. 2022;61:SB0802.
10. Qiu C, Xu Z, An Z, Liu J, Zhang G, Zhang S, et al. In-situ domain structure characterization of $Pb(Mg_{1/3}Nb_{2/3})O_3$–$PbTiO_3$ crystals under alternating current electric field poling. Acta Mater. 2021;210:116853.
11. Wan H, Luo C, Liu C, Chang W-Y, Yamashita Y, Jiang X. Alternating current poling on sliver-mode rhombohedral $Pb(Mg_{1/3}Nb_{2/3})O_3$–$PbTiO_3$ single crystals. Acta Mater. 2021;208:116759.
12. Qiu C, Wang B, Zhang N, Zhang S, Liu J, Walker D, et al. Transparent ferroelectric crystals with ultrahigh piezoelectricity. Nature. 2020;577:350–54.
13. Wang B, Li F, Chen LQ. Inverse domain-size dependence of piezoelectricity in ferroelectric crystals. Adv Mater. 2021;33:2105071.
14. Liu J, Qiu C, Qiao L, Song K, Guo H, Xu Z, et al. Impact of alternating current electric field poling on piezoelectric and dielectric properties of $Pb(In_{1/2}Nb_{1/2})O_3$–$Pb(Mg_{1/3}Nb_{2/3})O_3$–$PbTiO_3$ ferroelectric crystals. J Appl Phys. 2020;128:094104.
15. Kim HP, Zhang MH, Wang B, Wu H, Xu Z, Liu S, et al. Electrical de-poling and re-poling of relaxor-PbTiO3 piezoelectric single crystals without heat treatment. Nat Commun. 2024;15:6420.
16. Sun Y, Karaki T, Fujii T, Yamashita Y. Enhanced electric property of relaxor ferroelectric crystals with low AC voltage high-temperature poling. Jpn J Appl Phys. 2020;59:SPPD08.
17. Shpyrko OG. X-ray photon correlation spectroscopy. J Synchrotron Radiat. 2014;21:1057–64.
18. Xu J, Deng H, Zeng Z, Zhang Z, Zhao K, Chen J, et al. Piezoelectric performance enhancement of $Pb(Mg_{1/3}Nb_{2/3})O_3$–$0.25PbTiO_3$ crystals by alternating current polarization for ultrasonic transducer. Appl Phys Lett. 2018;112:182901.
19. Deng C, Ye L, He C, Xu G, Zhai Q, Luo H, et al. Reporting excellent transverse piezoelectric and electro-optic effects in transparent rhombohedral PMN–PT single crystal by engineered domains. Adv Mater. 2021;33:2103013.
20. Song K, Ma M, Hu Q, Qiao L, Zhao J, Qiu C, et al. Enhanced piezoelectric properties and domain morphology under alternating current electric field poled in [001]-oriented PIN–PMN–PT single crystal. J Appl Phys. 2022;132:114103.
21. Gorfman S, Bokov AA, Davtyan A, Reiser M, Xie Y, Ye ZG, et al. Ferroelectric domain wall dynamics characterized with X-ray photon correlation spectroscopy. Proc Natl Acad Sci U S A. 2018;115:E6680–89.
22. Yang T, Wang B, Hu JM, Chen LQ. Domain dynamics under ultrafast electric-field pulses. Phys Rev Lett. 2020;124:107601.
23. Liu Z, Meier AL, Wessels BW. Dynamic response of polydomain ferroelectric barium titanate epitaxial thin films and its field dependence. J Appl Phys. 2008;104:064115.
24. Li J, Lin PT, Wessels BW. Polarization reversal and backswitching dynamics in epitaxial $BaTiO_3$ thin films. J Appl Phys. 2009;106:054113.
25. Kim S, Gopalan V, Kitamura K, Furukawa Y. Domain reversal and nonstoichiometry in lithium tantalate. J Appl Phys. 2001;90:2949–63.
26. Liu YX, Thong HC, Cheng YYS, Li JW, Wang K. Defect-mediated domain-wall motion and enhanced electric-field-induced strain in hot-pressed $K_{0.5}Na_{0.5}NbO_3$ lead-free piezoelectric ceramics. J Appl Phys. 2021;129:024102.
27. Glaum J, Granzow T, Rödel J. Evaluation of domain wall motion in bipolar fatigued lead–zirconate–titanate: a study on reversible and irreversible contributions. J Appl Phys. 2010;107:104119.
28. Manjón-Sanz A, Culbertson CM, Hou D, Jones JL, Dolgos MR. Total scattering and diffraction studies of lead-free piezoelectric $(1-x)Ba(Zr_{0.2}Ti_{0.8})O_3$–$x(Ba_{0.7}Ca_{0.3})TiO_3$ deconvolute intrinsic and extrinsic contributions to electromechanical strain. Acta Mater. 2019;171:79–91.

29. Xing J, Mo M, Cheng Y, Tan Z, Zhu J. Decoding the piezo-contributions of potassium sodium niobate ceramics. J Phys Chem C. 2024;128:658–66.
30. Gao J, Hu X, Zhang L, Li F, Zhang L, Wang Y, et al. Major contributor to the large piezoelectric response in $(1-x)Ba(Zr_{0.2}Ti_{0.8})O_3-x(Ba_{0.7}Ca_{0.3})TiO_3$ ceramics: domain wall motion. Appl Phys Lett. 2014;104:252909.
31. Zhang S, Sherlock NP, Meyer RJ Jr., Shrout TR. Crystallographic dependence of loss in domain engineered relaxor-PT single crystals. Appl Phys Lett. 2009;94:162906.
32. Zhang MH, Zhang Q, Yu TT, Li G, Thong HC, Peng LY, et al. Enhanced electric-field-induced strains in (K, Na)NbO_3 piezoelectrics from heterogeneous structures. Mater Today. 2021;46:44–53.
33. Tagantsev AK, Cross LE, Fousek J. Domains in ferroic crystals and thin films. New York: Springer; 2010.
34. Madsen A, Leheny RL, Guo H, Sprung M, Czakkel O. Beyond simple exponential correlation functions and equilibrium dynamics in X-ray photon correlation spectroscopy. New J Phys. 2010;12:055001.
35. Otoničar M, Bradeško A, Salmanov S, Chung CC, Jones JL, Rojac T. Effects of poling on the electrical and electromechanical response of PMN–PT relaxor ferroelectric ceramics. Open Ceram. 2021;7:100140.

SUPPORTING INFORMATION

Additional supporting information can be found online in the Supporting Information section at the end of this article.

How to cite this article: Sun J-W, Fluerasu A, Xu Z, Liu S, Lee S-G, Jo W, et al. Enhanced domain dynamics in alternating current poled rhombohedral $Pb(Mg_{1/3}Nb_{2/3})O_3$–$PbTiO_3$ single crystals. J Am Ceram Soc. 2025;108:e20610. https://doi.org/10.1111/jace.20610